Planetary and Space Science 159 (2018) 17–27

Contents lists available at ScienceDirect

Planetary and Space Science

journal homepage: www.elsevier.com/locate/pss

Mars rotation determination from a moving rover using Doppler tracking data: What could be done?

Sebastien Le Maistre [a,*], Pascal Rosenblatt [b], Veronique Dehant [a], Jean-Charles Marty [c], Marie Yseboodt [a]

[a] Royal Observatory of Belgium, Brussels, Belgium
[b] ACRI-ST, Sophia-Antipolis, France
[c] Centre National d'Etudes Spatiales, Toulouse, France

A B S T R A C T

This paper is a case study providing some insights on what improvement could be achieved on the Mars Orientation and rotation Parameters (MOP) determination using radio tracking data from a moving rover. Thanks to high-performance mobility systems onboard new generation of rovers like *ExoMars 2020*, the position of the rover can be precisely known with respect to its previous position. This characteristic, together with the long life of the rovers and their steerable high-gain-antenna communication system, is shown here to provide an unexpected opportunity to improve the MOP determination. This paper presents the results of numerical simulations involving radio-science experiments between the moving rover and the Earth ground stations as well as between the rover and an orbiting spacecraft. The benefits of combining both links (direct-to-Earth and rover-orbiter) for the MOP determination is also assessed. The impacts of the spacecraft position accuracy as well as the frequency band used to communicate with it are quantified. It is shown that, after one Martian year of operation, the polar motion could be determined with 5 milliarcsecond (mas) of precision (formal error) from the rover-orbiter Doppler link, while it cannot be determined with usual equatorial lander-to-Earth radio link. This would allow for the first time the direct detection of the Chandler wobble amplitude in the polar motion of Mars, which is an important quantity to constrain the planet interior and atmospheric models. Although the moving rover Doppler data alone barely improve the current precision on the other MOP (like the length-of-day and nutation), a combination of those together with historical and future lander data would definitely help to fill gaps in the MOP signal and to decorrelate between the estimated parameters, thereby reducing the uncertainties in their determination.

1. Introduction

1.1. Geophysical interest

The knowledge of the interior structure of planets is fundamental to our understanding of their formation and evolution (e.g. Van Hoolst and Rivoldini (2014)). The planet's orientation and rotation variations can be used to deduce characteristics of the interior and of the dynamics of the fluid layers (e.g. Van Hoolst (2007)). The changes in Mars rotation rate are mostly due to exchanges of angular momentum between the atmosphere and the ice caps. Because of the presence of a normal mode called the Free Core Nutation (see Sec 3), the liquid core is expected to modify the periodic oscillations in the spin-axis orientation (called nutations). The secular drift (i.e. precession) of the spin axis allows determining the polar moment of inertia (MOI) of the whole planet, which quantifies the mass concentration towards the center and is a major constraint for models of the interior structure of planets. These are the reasons why improving the Mars rotation and Orientation Parameters (MOP) is considered by space agencies as high priority objective. End of 2018, NASA will land on the surface of Mars the *InSight* mission, carrying the RISE experiment (Folkner et al., 2012, 2018) and two years later, ESA, in collaboration with Roscosmos, will send the *ExoMars* (part 2) mission with the LaRa instrument (Dehant et al., 2009) on board of the surface platform. Both RISE (Rotation and Interior Structure Experiment) and LaRa (Lander Radio-science) are coherent transponders intended for radio tracking directly from the Earth. Although orbiters have been used to obtain variations in rotation/orientation of Mars from similar radio tracking data (e.g. Konopliv et al., (2006, 2011, 2016); Kuchynka et al., (2014)), landed probes are the best ones to study the rotation of their host (e.g. Folkner et al., (1997); Kuchynka et al., (2014); Le Maistre (2013)). Tied to the planet' surface, landers are definitely the most suitable probes because their motion in space is fully and only induced by the planet motion and deformation, both related to the physical properties of the planet. Rovers are less interesting at first glance because their motion on the planet's surface results in a larger displacement in space than the one induced by the planet rotation and orientation

* Corresponding author.
E-mail address: sebastien.lemaistre@oma.be (S. Le Maistre).

https://doi.org/10.1016/j.pss.2018.03.020
Received 4 August 2017; Received in revised form 30 March 2018; Accepted 31 March 2018
Available online 6 April 2018

variations that we are looking for. Therefore, if not precisely determined, the rover motion at the surface overwhelms the geophysical signal affecting the MOPs, explaining why the rover measurements have been discarded in the Mars rotation studies until now.

1.2. Radio-science historical concepts to measure the MOP

RISE and LaRa are radio-science experiments both dedicated to precisely measure the rotation and orientation of Mars. Their ability to improve our knowledge on the MOP and to provide some constraints on Mars physical parameters using a Direct-To-Earth (DTE) radio link from a fixed station at the surface of Mars has already been demonstrated through simulations (Le Maistre et al., 2012). More specific simulations about these two missions will be published in a near future (e.g. Folkner et al., (2018) for RISE). Other geodetic experiments with the same goals have been proposed in the past and sometimes deeply studied. For instance, in the beginning of the millennium, the *NetLander* mission (Harri et al., 1999) was planned to be launched in 2007 and to deploy four micro-stations on Mars' surface to better understand the atmosphere, the surface and the internal structure of the red planet (Barriot et al., 2001; Yseboodt et al., 2003; Rosenblatt et al., 2004). More recently, a very promising experiment for measuring the rotation of a celestial body has been proposed for the Moon (Gregnanin et al., 2012) and for Mars (Yseboodt et al., 2012). This again involves a network of landers (or rovers) tracked from the Earth with a configuration known as Same Beam Interferometry (SBI) (Kahn et al., 1992). This experiment is however not yet selected and will certainly not be sent to Mars before a decade or more.

1.3. Rationale of the MOP measurements from a moving rover

Still in order to improve the MOP estimates precision, we investigate here another kind of experiment involving a moving rover. Such an experiment has not been considered so far since the change in the rover location between tracking sessions has always been thought to overwhelm the rotational signal we are looking for. However, although less promising than the previously cited ones which are fixed at the surface, there are three good reasons to think that the experiment presented here is definitely worth investigating for the MOP determination.

First, it involves long-standing probes existing or arriving soon at Mars. Indeed, four rovers have already been landed on Mars: *Sojourner* (1997), *Spirit*, *Opportunity* and *Curiosity*. And two additional ones, *ExoMars 2020* ESA rover and *Mars 2020* NASA rover, will be launched to Mars in 2020. *Spirit* (2004–2010) and *Opportunity* (2004-), the twins Mars Exploration Rovers (MER) have been operating from Mars' surface for six and more than thirteen years respectively. *Curiosity* (2012-) already spend more than 5 years at the surface of Mars.[1] *ExoMars 2020* nominal mission duration is one Earth year and *Mars 2020* nominal mission duration is one Martian year, which is very long since the nominal mission duration is the minimum mission insured by the spatial agencies.[2]

The second asset lies in the very high performance of the mobility systems of the new generation of rovers (Winter et al., 2015). For instance, the *ExoMars 2020* rover resorts to an autonomous mobility system to access sites of scientific interest with minimal ground support. Such a system combines Guidance, Navigation and Control (GCN) subsystem and locomotion subsystems (see details on the hardware in Winter et al., (2015). These hardware, together with advanced algorithms, has been proven by Winter et al., (2015) to allow relative localisation of the rover (with respect to its initial position) with very high accuracy (cm level) even if the rover undergoes slippage due to sandy soil. It seems then reasonable to assume that such mobility system will permit to position the rover at a given time with a precision of $\leq$10-cm relatively to its previous position.

Finally, a third virtue of the proposed concept comes from the high performance of the telecommunication system onboard the rovers. Indeed, the rovers are all[3] equipped with telecommunication system allowing for X-band 2-way coherent Doppler tracking in DTE. Moreover, they all have steerable High Gain Antennas (HGA), allowing to point the radio beam toward the Earth without reorienting the rover. This is a very powerful system, which does not exist on the upcoming landers (LaRa uses low gain omnidirectional monopole antennas and RISE uses two directional medium gain horn antennas). It allows to communicate with the Earth within the maximum antenna performance region, any time when the Earth is in the rover' sky. This offers the opportunity to profusely collect radio-science measurements in a large diversity of geometric configurations (i.e. for different elevations and azimuths of the Earth during the tracking pass). It ensures also the best Doppler measurement accuracy possible since the transponder (thermal) noise, depending on the up- and down-link signal-to-noise ratio (e.g. Zuber et al., (2007)), is then minimised.

These three aspects (long-life time, mobility systems and steerable HGA) of the 2020 rover missions motivate the present study, since they provide a real opportunity to offset the negative impact of the displacement of the rover at the surface of the planet in the MOP determination.

We perform numerical simulations to assess the precision that can be obtained on the determination of the Mars rotation and orientation parameters by using radio links between a moving rover and the Earth and between the rover and a spacecraft in orbit around Mars. We evaluate the impact of different mission parameters in the determination of the MOP such as: the frequency band (X-band versus UHF), the precision in rover positioning at surface (with or without mobility system), the nature of the radio link (DTE or via orbiter), and the precision in the relay-spacecraft orbit calculation (well-known versus meter level). The results of our simulations with a rover are compared to similar ones with a fixed station on Mars' surface (see Le Maistre et al., (2012) for details on the DTE link from a lander). We also take a look at the performance of a "triangular configuration", involving rover-orbiter, rover-Earth and orbiter-Earth radio links simultaneously. All the simulations have been performed using the GINS (Géodésie par Intégrations Numériques Simultanées) software. This software has been developed by Center National d'Etudes Spatiales (CNES) and further adapted at the Royal Observatory of Belgium to allow for planetary applications involving surface landers and rovers (Le Maistre et al., 2012; Le Maistre, 2013).

The simulation setup (Sec. 2) and the Mars rotation model (Sec. 3) are presented first, followed by the simulation results on the moving rover positions determination (Sec. 4). Section 5 provides the MOP determination precision that can be achieved with a moving rover compared to those obtained with a lander, fixed at the surface of Mars. We then present the advantages of having a triangular configuration in the determination of the rotation parameters (Sec. 6). The conclusions are summarised in Section 7.

2. Simulation setup

Taking as a reference the lander case which has been deeply studied in the past, we compare hereafter the simulation results obtained with the moving rover to those obtained with a lander. We choose to locate both the lander and the rover near the *Opportunity* landing site, i.e. at $\lambda =$

[1] Note that *Spirit* and *Opportunity* data has been used only when the rovers were fixed at the surface of Mars (Le Maistre, 2013; Kuchynka et al., 2014). *Curiosity* never stopped and no radio-science campaign has been performed with it yet. Since the proposed analysis was never performed before, no radio-science campaign has been considered until now, while the rovers were keeping moving.

[2] All the payloads are build to survive at least over that time, but the effective mission life time is often much longer than the nominal duration.

[3] Except for *Sojourner*, which was a technology demonstrator.

Table 1
Tracking characteristics of each link for a 700 days mission duration as consider in this paper. RDTE and LDTE stand for Lander and Rover DTE, respectively.

Measurement type	Frequency band	Measurement noise	Session duration	Session recurrence	Number of sessions	Total data points
RDTE	X-band	0.05 mm/s@60s	10 min.	1 day	700	7000
ROL	X-band	0.05 mm/s@60s	10 min.	1 day	700	7000
ROL	UHF	0.30 mm/s@60s	10 min.	1 day	700	7000
LDTE	X-band	0.05 mm/s@60s	45 min.	3.5 days	200	9000
LOL	X-band	0.05 mm/s@60s	20 min.	7 days	100	2000
LOL	UHF	0.30 mm/s@60s	20 min.	7 days	100	2000

354°E of longitude and $\varphi = 2$°S of latitude. X-band DTE Doppler data from the lander are created exactly as in Le Maistre et al., (2012) (twice a week, during 45 min, over 700 days, with a line-of-sight elevation angle between [20°,40°]). The lander is tracked once a week during 20 min (as foreseen for late *NetLander* mission) from the orbiter. The rover tracking is repeated every day during 10 min (as expected for *ExoMars* rover) either from the Earth (2-way DTE in X-band) or from the orbiter. Both Rover-Orbiter-Link (ROL) and Lander-Orbiter-Link (LOL) are created in UHF— and X-band. Each Doppler data in X-band is superimposed with a white noise of 0.05 mm/s at 60 s of integration time and UHF Doppler data are produced with a six times larger noise of 0.3 mm/s at 60 s (see Table 1). DTE, LOL and ROL are all generated using the same Mars rotation model described in the following section.

We consider a quasi-polar (89° of inclination) and circular orbit (typical for Mars orbiting spacecraft apart from *MEX*, *TGO* and *MAVEN*) with a semi-major axis equal to 3900 km (i.e. 500 km of altitude). A well-known orbiter trajectory, only degraded at the centimeter level by the X-band data noise used to reconstruct the orbit, is considered for comparison with the meter level of orbit accuracy. The well-known orbit is used to point out the best performance we can theoretically obtain on the MOP estimates from the datasets considered in this study. The other orbit is chosen as baseline in these simulations because the typical total orbit overlap error of the current martian satellites is about 1 m (see for instance Marty et al., (2009); Konopliv et al., (2011)). The 1 m-degraded orbit is produced by perturbing the gravity field when reconstructing the orbit from the simulated X-band Doppler tracking data of the spacecraft. Basically, the 80×80 gravity model used to generate the data is truncated to degree and order 65 when fitting the parameters. In our simulations we consider arcs of 7-days length. The orbiter initial states (IS) are systematically estimated along with the other parameters (MOP and lander/rover positions, see next section). However, because of the gravity field truncation, the IS adjustment can only reduce the orbit errors to ± 1 m, which is the exact purpose of the manipulation. The overlaps between the orbit used during the estimation process and the orbit used to create the LOL/ROL data are shown in Fig. 1 for the first three arcs over the 100 ones used in our simulation. These overlaps are going from -1.2 m to $+1$ m on the along-track (tangential to the orbit) and remain below 20 cm (8 cm) for the normal (radial) component. In RMS, these errors are at the $10 \times 50 \times 3$ cm level in RTN (Radia, Tangential, Normal), which is in good agreement with those computed by Konopliv et al., (2011) on the real orbiter data (see their Fig. 8). Since the study here does not focus on the spacecraft precise orbit determination (POD), and because the order of magnitude of the error introduced in our orbit along each RTN direction is well inline with the current POD performances, we do not introduce more realistic perturbations on the orbiter trajectory.

It is worth to also mention that no data timing error are introduced in the LOL/ROL, whereas one could expect some because of the non-perfect stability of the clock onboard the spacecraft.[4] In that sense, the simulations shown here for LOL/ROL are a bit optimistic since one could have to also adjust a pair of clock parameters. Typical clock parameters are the "clock offset error", "clock rate offset" and "clock drift" which basically are the coefficients of a polynomial of degree two. Preliminary simulations showed that such additional clock parameters induce a lost of precision in the nutation parameter estimates of about 2–5% relative to the precisions shown in the following sections of the paper. Such degradation in the MOP determination does not change the conclusions of the present study.

[4] The two-way DTE measurements do not suffer such a timing error because the timestamp is provided by active hydrogen maser of the Earth ground stations.

3. Mars rotation model and parameters setup

The rotation model of Mars allows to transform a vector $\vec{r}_{in}$ expressed in the inertial system related to the Mars Mean Orbit (MMO) of a given epoch (t_0) into the vector $\vec{r}_{bf}$ in the body-fixed rotating frame tied to the planet (both frames being centred on Mars). At J2000 epoch, the Mars mean orbit reference frame, denoted MMO2000, is such that the MMO2000 z-axis is the normal of the Mars mean orbital plane of J2000 (at midday), the x-axis is along the ascending node A (see Fig. 2) of the Mars mean orbit of J2000 on the International Celestial Reference Frame (ICRF) and the y-axis completes the orthogonal right triad. The z-axis of the Mars-fixed reference frame is the direction of spin when the polar motion of Mars is null. The x-axis cut the prime meridian at its intersection with the true equator of date (point E in Fig. 2), and the y-axis completes the orthogonal right triad.

As shown on Fig. 2, I is the inclination of the Mars true equator of date with respect to the Mars mean orbital plane at J2000 and ψ locates the longitude of the node D between those two planes (corresponding to the true equinox of Mars $\gamma_{t_{Mars}}$) counted from the node A. The sidereal angle ϕ corresponds to the spin angle of the planet with respect to the stars. It gives the position of the prime meridian of Mars and is measured along the true equator of date starting from the node of the true equatorial plane of date (D). X_p and Y_p are two rotation angles characterising the planet polar motion. They allow passing from the frame tied to the rotation axis to the frame tied to the planet. All these angles can be decomposed as follows:

$$I = I_0 + \dot{I}_0(t - t_0) + \sum_{m=1}^{6}\left(I_m^c \cos\left(\frac{2\pi}{T_m}t\right) + I_m^s \sin\left(\frac{2\pi}{T_m}t\right)\right), \tag{2}$$

$$\psi = \psi_0 + \dot{\psi}_0(t - t_0) + \sum_{m=1}^{6}\left(\psi_m^c \cos\left(\frac{2\pi}{T_m}t\right) + \psi_m^s \sin\left(\frac{2\pi}{T_m}t\right)\right), \tag{3}$$

$$\Phi = \phi_0 + \dot{\phi}_0(t - t_0) + \sum_{m=1}^{2}\left(\phi_m^c \cos\left(\frac{2\pi}{T_m}t\right) + \phi_m^s \sin\left(\frac{2\pi}{T_m}t\right)\right) - \psi_{nut}\cos I, \tag{4}$$

$$X_p = \sum_{m=1}^{2}\left(X_m^c \cos\left(\frac{2\pi}{T_m}t\right) + X_m^s \sin\left(\frac{2\pi}{T_m}t\right)\right) + \left(X_{cw}^c \cos\left(\frac{2\pi}{T_{cw}}t\right) + X_{cw}^s \sin\left(\frac{2\pi}{T_{cw}}t\right)\right), \tag{5}$$

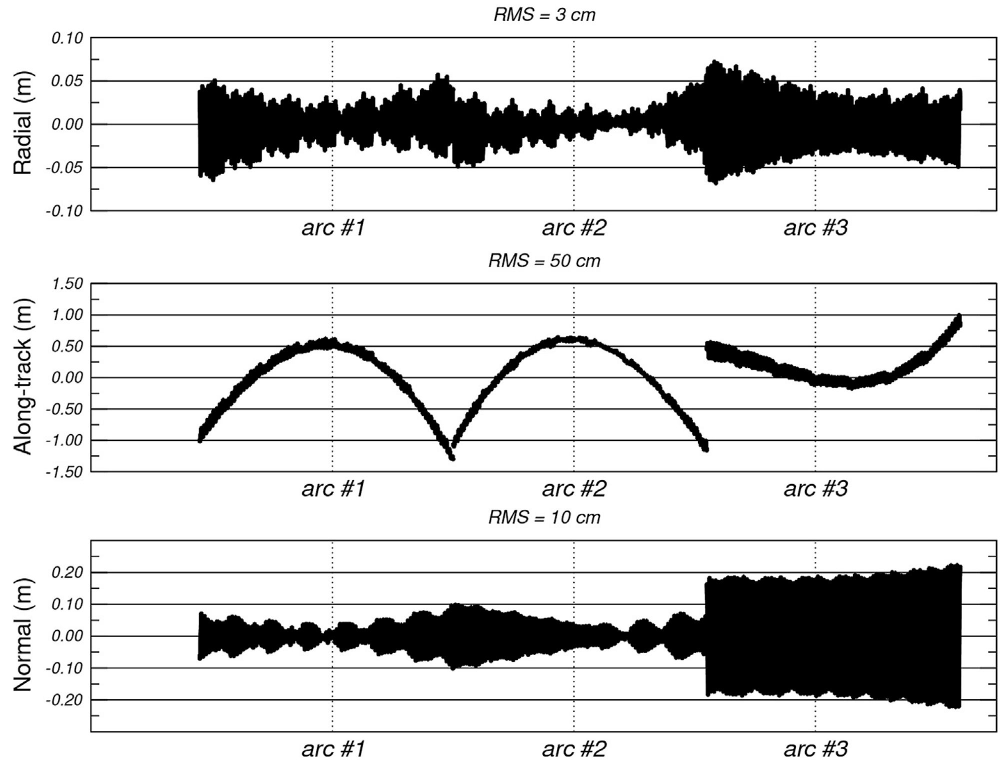

Fig. 1. Orbit overlap of three consecutive arcs of one week length each for the radial (top), along-track (middle), and normal (bottom) to the orbit plane directions.

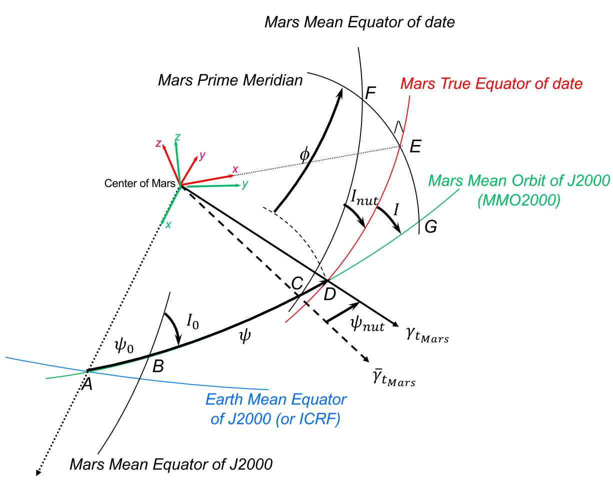

Fig. 2. Reference frames and Mars orientation angles for conversion between Mars mean orbit reference frame of J2000 (in green) and Mars body-fixed reference frame of date (in red).

$$\vec{r}_{bf} = R_y(-X_p)R_x(-Y_p)R_z(\phi)R_x(-I)R_z(\psi)\vec{r}_{in}. \quad (1)$$

The rotation of Mars is modelled with five successive elementary rotations (see further details in Le Maistre et al., (2012). (For interpretation of the references to colour in this figure legend, the reader is referred to the Web version of this article.)

$$Y_p = \sum_{m=1}^{2}\left(Y_m^c\cos\left(\frac{2\pi}{T_m}t\right)+Y_m^s\sin\left(\frac{2\pi}{T_m}t\right)\right)+\left(Y_{cw}^c\cos\left(\frac{2\pi}{T_{cw}}t\right)+Y_{cw}^s\sin\left(\frac{2\pi}{T_{cw}}t\right)\right). \quad (6)$$

I_0 and ψ_0 (*AB* on Fig. 2) are, respectively, the obliquity and longitude of the node of the Mars mean equator at epoch (t_0). $\dot{I}_0$ is the secular change in the Mars obliquity and $\dot{\psi}_0$ is the precession rate of Mars spin axis. I_{nut} and ψ_{nut} on Fig. 2 are the nutation in obliquity and longitude, respectively. They correspond to the periodic variations (i.e. series) of sine amplitudes, I_m^s,ψ_m^s, and cosine amplitudes, I_m^c,ψ_m^c, in Eqs. (2) and (3). $\dot{\phi}_0$ is the constant diurnal angular velocity of Mars and $\phi_m^{c,s}$ are the amplitudes of the seasonal variations of the spin angle, also called hereafter the Length-Of-Day (LOD) variations amplitudes.[5] The forcing periods T_m are the harmonics of Mars orbital periods. T_1 (i.e. m = 1) is the annual period of 687 terrestrial days and the next harmonic periods (m≥2) correspond to the semi-annual (343.5d), the ter-annual (229d), the quarter-annual (171.7d), etc. An additional frequency denoted by the subscribe *cw* is introduced for the polar motion (Eq. (5) and (6)). It corresponds to the wobbles associated to the Chandler mode of Mars (e.g. Van Hoolst et al., (2000b)). The period T_{cw} of this signal is uncertain but is expected to be around 200 days (Van Hoolst et al., 2000a,b). The amplitudes of the complex prograde (p_m) and retrograde (r_m) nutation terms considered in the present paper are related to the nutation amplitudes (Defraigne et al., 1995) in obliquity ($I_m^{c,s}$) and longitude ($\psi_m^{c,s}$) by:

$$p_m e^{\frac{2i\pi}{T_m}t} + r_m e^{-\frac{2i\pi}{T_m}t} = I_m^c\cos\left(\frac{2\pi}{T_m}t\right) + I_m^s\sin\left(\frac{2\pi}{T_m}t\right) + i\sin I_0\left(\psi_m^c\cos\left(\frac{2\pi}{T_m}t\right) + \psi_m^s\sin\left(\frac{2\pi}{T_m}t\right)\right), \quad (7)$$

where $i^2 = -1$. A fluid core modifies the prograde and retrograde terms according to the following equations (Sasao et al., 1977):

$$p_m^{'} = p_m\left(1 + F\frac{T_{FCN}}{T_{FCN}-T_m}\right), \quad (8)$$

[5] Note that "LOD" to describe $\phi_m^{c,s}$ is a misnomer since the former is assimilated to a time and the latter to an angle. Both are nevertheless related by $LOD_m^c = 4\pi^2/(\dot{\phi}_0^2 T_m)\phi_m^s$ and $LOD_m^s = -4\pi^2/(\dot{\phi}_0^2 T_m)\phi_m^c$.

$$r_m^{'} = r_m\left(1 + F\frac{T_{FCN}}{T_{FCN} + T_m}\right), \quad (9)$$

where the primed quantities are the amplitudes of nutation for a non-rigid planet and F and T_{FCN} are the core momentum factor and the Free-Core-Nutation (FCN) period. They are both related to interior properties like the moments of inertia and dynamical flattenings of the whole planet and of the fluid core, as well as Love numbers characterising their deformation.

The truth model used to create the simulated Doppler data is shown in Table 2. Among all the MOP of the truth model, we only estimate a subset of parameters. Basically, all the simulations performed hereafter are simultaneously estimating the lander/rover position coordinates, the LOD variations amplitudes (annual and semi-annual) and the nutation amplitudes (annual, semi-annual and ter-annual). Simulations involving ROL/LOL measurements also estimate the polar motion parameters. The other MOPs are maintained fixed (see Table 2) because considered as well-known (their uncertainty has a signature in the Doppler measurements well below the noise level).

The rotational parameters are perturbed as in Le Maistre et al., (2012). A priori constraints on each ΔLOD (i.e. spin angle) parameter are set to 20% of the truth model. The a priori constraints in nutation amplitudes are set to 200% of the largest possible contribution of a liquid core, which is computed from Eqs. (8) and (9) assuming $T_{FCN} = -230$ days and $F = 0.12$. Only the trigonometric amplitudes of nutation are estimated herein contrary to Le Maistre et al., (2012) who also considered scenarios where F and the FCN frequency were the estimated nutation parameters. Also differently from Le Maistre et al., (2012) the polar motion parameters, still perturbed at the 100% level of the truth model from Van den Acker et al., (2002), are estimated together with all other parameters (MOP plus lander/rover coordinates) when dealing with the LOL/ROL signals. The DTE Doppler data from an equatorial Martian station are insensitive to the polar motion signal (Le Maistre et al., 2012; Yseboodt et al., 2017). This is not the case with LOL/ROL data, which are sensitive to the polar motion because of the Doppler geometry offered by the polar orbit of the spacecraft. Indeed, as one can see on Fig. 3 an equatorial lander communicating with a polar orbiter is a good configuration to observe the polar motion signal, whose signature reach then 3 mm/s RMS in the Doppler, assuming an amplitude of about 65-cm at the surface. Annual and semiannual polar motion parameters a priori constraints are fixed to 10 mas (which is larger than 100% of the truth model amplitudes, see Table 2). The amplitudes of the Chandler wobbles (i.e. $X^c_{cw}, X^s_{cw}, Y^c_{cw}, Y^s_{cw}$) are expected to be larger than the annual and sub-annuals amplitudes of the polar motion (Van den Acker et al., 2002) and are arbitrarily set to ~33 mas[6] while their a priori constraints are taken equal to 100% of the values to retrieve (see Table 2). Finally, a priori constraints on the lander cartesian coordinates are 200 × 200 × 200 km. We consider a rover moving at the surface of Mars by hundreds of meters every week. Each of its successive locations are expected to be known at the 10-cm level of precision relatively to its previous position.

4. Determination of the moving rover positions

Expecting a mobility system is available, we assume also that the first rover location ($\overrightarrow{X}_0$) is known at the 10-cm level. Such a 10-cm of accuracy is challenging but could be reached from a few days commissioning phase during which 1) the rover would be fixed and tracked from the Earth and from an orbiting spacecraft simultaneously, 2) panoramic images would be used to locate the lander relative to surface features observed in images, 3) refined method (Le Maistre, 2016) would be

[6] Note that the amplitude values of the Chandler wobbles (or of any other MOP amplitudes) have actually no influence on the precision with which one can estimate them.

Table 2
Mars rotation model used as the truth model to create the synthetic Doppler data, along with the a priori constraints on the MOP estimated in our simulations. Angles at epoch (I_0, ψ_0, ϕ_0), rates ($\dot{I}_0, \dot{\psi}_0, \dot{\phi}_0$) and spin angle amplitudes are from Konopliv et al. (2016). The amplitudes of the truth model of nutation are computed from the model of rigid nutation of Roosbeek (1999) modulated by a liquid core of FCN period equal to −240 days and F equal to 0.07 according to Eqs. (8) and (9). The polar motion nominal amplitudes are from Van den Acker et al. (2002), while the Chandler wobbles amplitudes are arbitrarily chosen.

Parameter	Symbol	Nominal (Truth model)	a priori constraint
Obliquity at t_0 (deg)	I_0	25.189	fixed
Longitude at t_0 (deg)	ψ_0	81.97	fixed
Prime meridian at t_0 (deg)	ϕ_0	133.386	fixed
Obliquity rate (mas/year)	$\dot{I}_0$	−2.0	fixed
Precession rate (mas/year)	$\dot{\psi}_0$	−7608.3	fixed
Rotation rate (deg/day)	$\dot{\phi}_0$	350.891985307	fixed
1-annual cosine spin angle (mas)	ϕ^c_1	481	100
1/2-annual cosine spin angle (mas)	ϕ^c_2	−103	25
1-annual sine spin angle (mas)	ϕ^s_1	−155	35
1/2-annual sine spin angle (mas)	ϕ^s_2	−93	20
1-annual prograde nutation (mas)	p_1	102	5
1/2-annual prograde nutation (mas)	p_2	498	40
1/3-annual prograde nutation (mas)	p_3	108	11
1/4-annual prograde nutation (mas)	p_4	18	fixed
1/5-annual prograde nutation (mas)	p_5	3	fixed
1/6-annual prograde nutation (mas)	p_6	0.5	fixed
1-annual retrograde nutation (mas)	r_1	137	14
1/2-annual retrograde nutation (mas)	r_2	18	7
1/3-annual retrograde nutation (mas)	r_3	5	185
1/4-annual retrograde nutation (mas)	r_4	1	fixed
1/5-annual retrograde nutation (mas)	r_5	0	fixed
1/6-annual retrograde nutation (mas)	r_6	0	fixed
1-annual cosine polar motion (mas)	X^c_1	2	10
1/2-annual cosine polar motion (mas)	X^c_2	−8	10
Chandler wobble cosine (mas)	X^c_{cw}	33	33
1-annual sine polar motion (mas)	X^s_1	−2	10
1/2-annual sine polar motion (mas)	X^s_2	−4.5	10
Chandler wobble sine (mas)	X^s_{cw}	33	33
1-annual cosine polar motion (mas)	Y^c_1	−5.5	10
1/2-annual cosine polar motion (mas)	Y^c_2	−4	10
Chandler wobble cosine (mas)	Y^c_{cw}	33	33
1-annual sine polar motion (mas)	Y^s_1	−10	10
1/2-annual sine polar motion (mas)	Y^s_2	−0.5	10
Chandler wobble sine (mas)	Y^s_{cw}	33	33

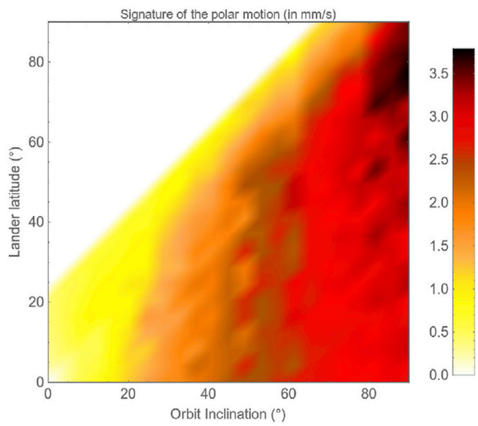

Fig. 3. Polar Motion (PM) signature in the LOL/ROL Doppler observable as a function of the lander/rover latitude and of the orbiter inclination. The drawn quantity is the quadratic mean of the signature temporal series over one Martian year. Doppler unit is mm/s. The spacecraft has a precessing orbit at 500 × 500 km altitude. The lander longitude is 354°.

applied to also constrain the Z coordinate (along the spin axis) which is otherwise difficult to infer from DTE Doppler data (Le Maistre et al., 2012). The a priori knowledge coming from the mobility system gives way to "continuity" constraints (or relative constraints), meaning that the constraints are relative to the previous position of the rover. These constraints are introduced into our software as follows:

$$\overrightarrow{X}_i = \overrightarrow{X}_{i-1} + \delta\overrightarrow{X}_i \pm \overrightarrow{\sigma_{X_i}}, \tag{10}$$

where $\overrightarrow{X}_i$ is the i^{th} position vector of the rover at which it has been tracked and $\delta\overrightarrow{X}_i$ is the i^{th} displacement performed by the rover between two positions where telecommunication operation have been carried out. The $\delta\overrightarrow{X}_i$ quantity will be provided by the mobility system with its associated uncertainty $\overrightarrow{\sigma_{X_i}} \simeq (10, 10, 10)^t$ cm, where the superscript t indicates the transposed of this line vector to produce a column vector as needed. It must be mentioned that dealing with a moving station with respect to the surface of the planet amounts in practice to deal with a network of landers, close to each others, that do not communicate simultaneously and that have a very short life time. Hereafter we estimate the MOP and rover coordinates every week over 700 days of mission duration. After a week of operation, the rotational parameters are estimated together with the 3 coordinates of the first position of the rover. At the end of the considered mission duration (i.e. after 100 weeks), we have 3 × 100 position parameters to estimate in addition to the MOP. Each rover position provides one normal matrix depending on the MOP (global parameters) and on its own position parameters (local parameters). These 100 normal matrices have to be stacked together to solve for the global parameters.

Fig. 4 shows the 1σ post-fit uncertainties obtained with 2-way DTE data in X-band and LOL/ROL data in UHF and in X-band. Thanks to the continuity constraints (Eq. (10)), we succeed to estimate each rover successive position from DTE measurements with a precision comparable to those of a lander, while the uncertainties in the rover coordinates achieved with ROL data and continuity constraints are more than one order of magnitude larger than those reached using LOL data for the lander coordinates.

Fig. 4a exhibits a comparison between the X, Y and Z estimated precision from LOL observable with a spacecraft positioned very accurately (centimeter level) and realistically (meter level). Roughly, the lander coordinates are estimated 10 times better if errors on the orbit are at centimeter level instead of meter level. Fig. 4a also shows that LOL estimates are better than DTE ones after ~350 days. This corresponds to half of a Martian year, which is the minimum duration needed to start improving the annual signals in the rotation (see Fig. 5a). The first 350-days estimated uncertainties are mostly driven by the a priori constraints. A comparison between links ability to estimate parameters within this first period is not relevant.

The rover precision in X and Y are about 10 times better with

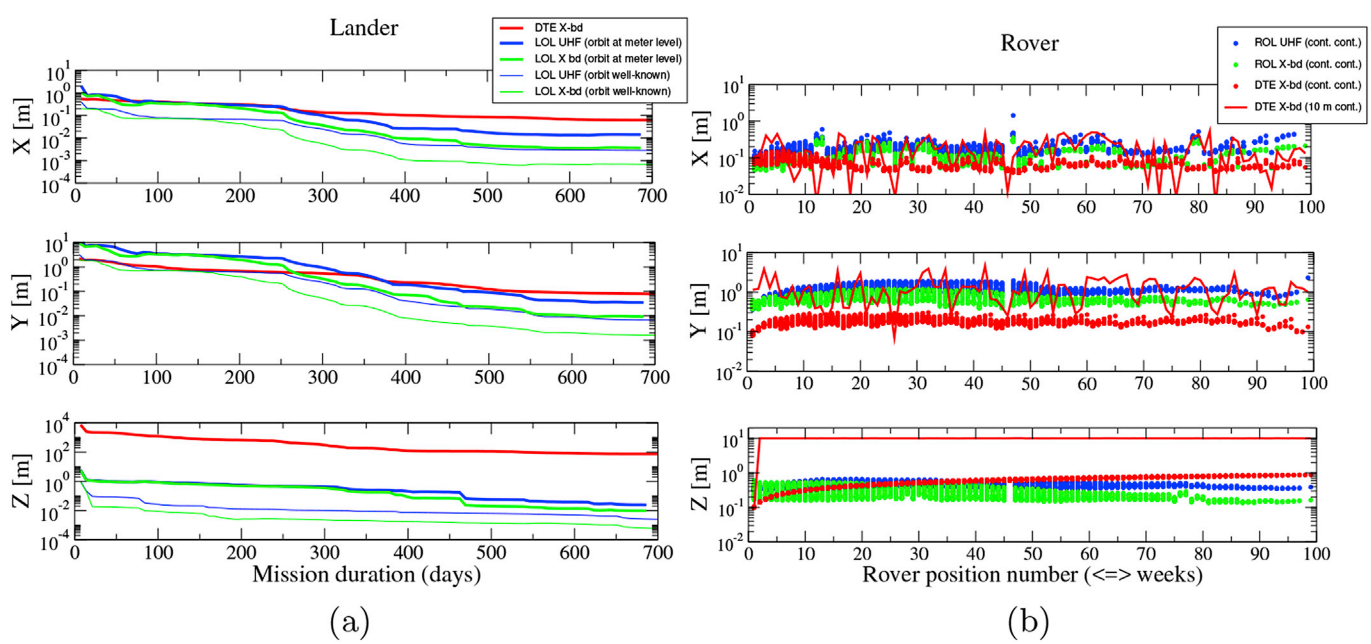

Fig. 4. Uncertainties in the coordinate estimates from Doppler tracking of a lander (a) and of a rover (b) as a function of the mission duration. 1σ uncertainties obtained using 2-way DTE data in X-band are in red. 1σ uncertainties obtained from LOL/ROL data are in blue when using UHF-band and are in green when using X-band. Thin and thick lines in lander's graphs show precision with spacecraft orbit at centimeter (ideal case) and meter level (realistic case) of accuracy, respectively. Rover coordinates precisions have been obtained using continuity constraints (*cont. cont.* with dots). Red solid lines in rover plots are DTE uncertainties using 10-m of a priori constraints (*10 m cont.*) on X,Y and Z, instead of the continuity constraints. (For interpretation of the references to colour in this figure legend, the reader is referred to the Web version of this article.)

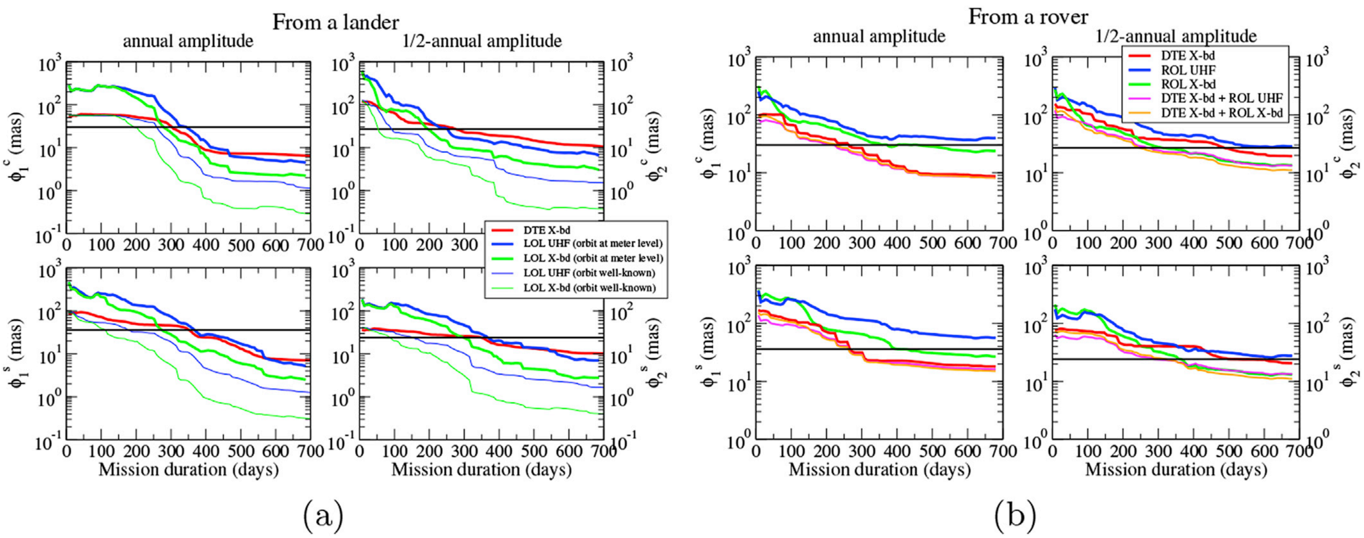

Fig. 5. Uncertainties in the seasonal rotation variation amplitude estimates from Doppler tracking of a lander (a) and of a rover (b) as a function of the mission duration. 1σ uncertainties obtained using 2-way DTE data in X-band are in red. 1σ uncertainties obtained from LOL(a)/ROL(b) data are in blue when using UHF-band and are in green when using X-band. Black horizontal lines represent the current 3σ uncertainties on each amplitude (Konopliv et al., 2016). Thin and thick curves in lander's graphs show precision with spacecraft orbit at centimeter and meter level of accuracy, respectively. Magenta and orange curves in rover's graphs show triangular configuration precisions for DTE plus UHF-ROL and DTE plus X-band-ROL, respectively (see Sec. 6). Rover uncertainties are obtained with continuity constraints in rover coordinates retrieval. (For interpretation of the references to colour in this figure legend, the reader is referred to the Web version of this article.)

continuity constraints than with 10-m constraint (only DTE 10-m uncertainties are displayed on Fig. 4b for readability, but ROL solutions present similar behavior). It is interesting to note that the 10-m a priori constraint still allows for an X,Y determination one or two order of magnitudes better than the constrain itself (red solid curves in Fig. 4b). The cumulative effect of the relative errors in the rover positioning is partially compensated by the systematic adjustment of the coordinates of each rover intermediate location. Only Z, in the DTE case, still suffers of a stacking of errors since the DTE data are not sensitive to Z and thus do not compensate for the cumulative errors. This is clearly shown in bottom panel of Fig. 4b, where the red-dotted curve increases over 700 days in a logarithmic way. Nevertheless, Z is retrieved with a precision still better than 1 m after one Martian year of DTE tracking thanks to the continuity constraints. Due to the rover motion at the surface of Mars, three additional parameters have to be estimated every time the rover location changes and communicates with an Earth ground station or the orbiter. Since we estimate the MOP and rover coordinates every week over 100 weeks, the first position is estimated 100 times in all, whereas the last position is estimated only once, which explains the peculiar aspect of the uncertainties plotted in Fig. 4b.

5. MOP determination with a moving rover

Together with the rover positions, we estimate the MOP. Fig. 5 displays the formal errors (or uncertainties) of the annual (ϕ_1^c and ϕ_1^s) and semiannual (ϕ_2^c and ϕ_2^s) amplitude estimates of the length-of-day variations. Despite the continuity constraints on the rover positions, the uncertainties in the rover ΔLOD amplitude estimates remains too large to significantly improve our current knowledge on the seasonal rotation variations of Mars (see Fig. 5b). ROL and DTE radio links from a rover provide comparable precision on ΔLOD, even if DTE appears a bit more efficient to precisely measure the annual rotation variation signal. Indeed, one can see on Fig. 5b (red curve) that the rover DTE might be able to provide some helpful information on ϕ_1^c by reducing the current uncertainty on this parameter (shown in black in the figure).

In DTE, lander and rover provide similar ΔLOD estimate precisions after one Martian year of mission (see red curves in Fig. 5). The factor of two better in the DTE lander case with respect to the DTE rover case is partly due to the larger number of data points in the lander case (90 min per week) than in the rover case (70 min per week) and mostly due to the larger number of parameters estimated in the rover case (three estimated coordinates per week) than in the lander case (three estimated coordinates in all).

The large difference between LOL and ROL estimated uncertainties (see Fig. 5) can not be explained by the difference of data points, which is this time favorable to the rover (20 min per week for the lander against 70 min per week for the rover). It can not be totally attributed neither to the increased number of correlations due to the increased number of estimated parameters in the rover case because, if so, the DTE red solutions would have been affected similarly.[7] The better estimation with LOL than with ROL (see blue and green curves in Fig. 5) is most likely due to the fact that the main advantage of the LOL scenario does not apply in the ROL scenario. Indeed, LOL is very powerful (also with respect to DTE) because of the various Doppler geometry (i.e. change in the line-of-sight directions) offered by the fast-varying position of the orbiter in the lander sky. Such a richness of the Doppler geometry does not exist in the rover case since each rover location only sees a small number of orbiter passes with respect to the lander which stands 700 days at the same location. Such a rich Doppler geometry explains why the LOL Doppler measurements in X-band (green curves in Fig. 5a) allow to estimate ϕ with a precision three times better than those obtained from DTE measurements. The latter advantage of X-band-LOL with respect to DTE is mitigated when LOL is performed in UHF (blue curves in Fig. 5a). The six time noiser measurements of the UHF-LOL with respect to X-band-DTE is partly responsible for this mitigation, which leads to similar precision in ϕ in DTE and UHF-LOL data after 300 days of observation.

Note that the LOL precisions are one order of magnitude better if errors on the orbit are at centimeter level instead of the current meter level of accuracy. This is also true in the nutation amplitude estimated precisions as shown on Fig. 6 for the special case of the semiannual prograde (p_2) and terannual retrograde (r_3) amplitudes (i.e. for the most interesting amplitudes to detect the liquid core signature in the rotation of Mars, see Le Maistre et al. (2012)). Fig. 6 shows that the mobility system would allow for a nutation determination with rover not much

[7] Unless DTE is a very powerful geometry to decorrelate the parameters, which is unlikely.

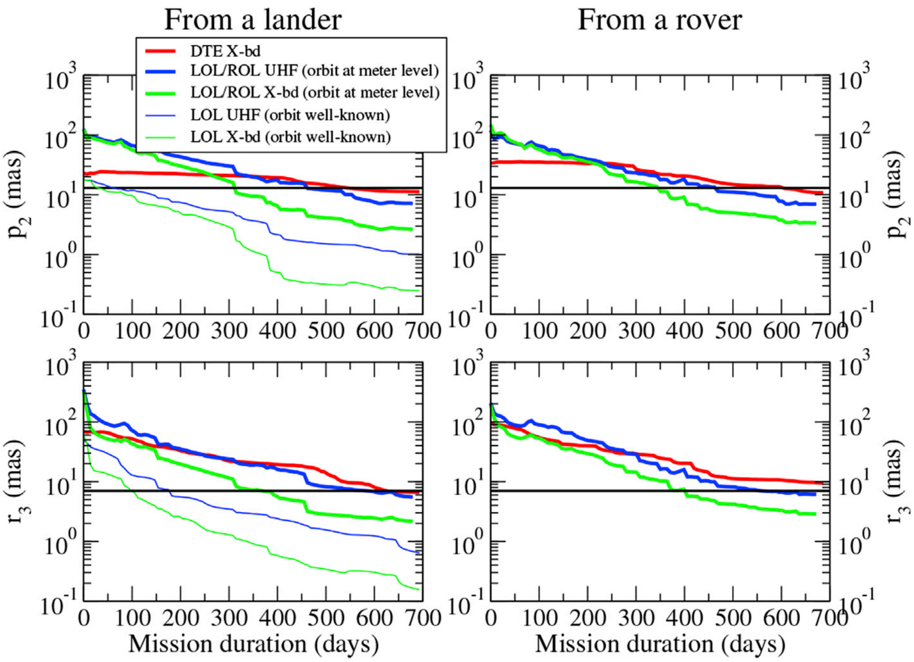

Fig. 6. Uncertainties in the nutation semiannual prograde and terannual retrograde amplitude estimates from Doppler tracking of a lander (left panels) and of a rover (right panels) as a function of the mission duration. 1σ uncertainties obtained using 2-way DTE data in X-band are in red. 1σ uncertainties obtained from LOL (left panels) and ROL (right panels) data are in blue when using UHF-band and are in green when using X-band. Black horizontal lines correspond to the amplifications due to liquid core FCN period equal to -240 days (and $F = 0.07$). Thin and thick lines in lander's graphs (i.e. left panels) show precision with spacecraft orbit at centimeter and meter level of accuracy, respectively. Rover uncertainties are obtained with continuity constraints in rover coordinates estimates. (For interpretation of the references to colour in this figure legend, the reader is referred to the Web version of this article.)

worse than using lander data and which could permit to detect the liquid core signature after more than 400–500 days of mission if the FCN period is equal to -240 days or is closer to the terannual forcing period (-229 days).

Fig. 7 Points out the impact of the rover location a priori knowledge on the determination of the MOP with DTE Doppler data. Only ϕ_2^c is displayed here, but all MOP estimates behave similarly. In addition to the formal errors (also called here uncertainties), this figure displays the true errors, which are the absolute differences between the estimated value of ϕ_2^c and its truth value reported in Table 2. If X, Y and Z coordinates of each stop location of the rover are a priori known with 10 m of error and estimated together with the MOP, taken ± 10 m of a priori constraints on each coordinate, then the MOP can not be retrieved (violet curve). When a priori constraints are at the 10-cm level (red curve), the determination

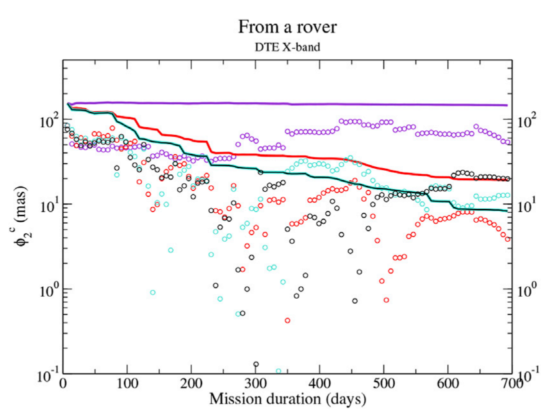

Fig. 7. True errors (open circles) and uncertainties (solid lines) in the semi-annual cosine amplitude estimates of the seasonal rotation variation (ϕ_2^c) from X-band 2-way DTE Doppler tracking of a rover as a function of the mission duration using different a priori errors and constraints on the rover coordinates: violet and red solutions are obtained with a priori errors and constraints equal to 10-m and 10-cm, respectively. Turquoise and black solutions of ϕ_2^c are obtained by fixing the rover position to its correct position and to a 10-cm misplaced position, respectively. Note that black and turquoise uncertainties are superimposed. (For interpretation of the references to colour in this figure legend, the reader is referred to the Web version of this article.)

is similar to the one we get with the continuity constraints since in the latter case we systematically estimate the rover position, which compensate for the stacking effect inherent in the continuity-constraints method. This figure also shows that a systematic error equal to 10-cm on each rover coordinate (black curve) does not significantly impact the MOP determination with DTE Doppler data from a moving rover since the precisions obtained then are equivalent to the ideal case of a well-positioned rover (turquoise curve).

The variation of the lander/rover position ($\vec{r} = \{d \cos\varphi \cos\lambda; d \cos\varphi \sin\lambda; d \sin\varphi\}$) due to Polar Motion (PM) can be expressed in a body-fixed reference frame as:

$$\Delta\vec{r} = \vec{r} - R_y(Y_p) R_x(X_p) \vec{r}, \tag{11}$$

$$= \{X_p d \sin\varphi \, ; \, -Y_p d \sin\varphi \, ; \, d \cos\varphi(-X_p \cos\lambda + Y_p \sin\lambda)\}, \tag{12}$$

where φ is the rover latitude, λ is its longitude and d is the distance of the rover to the center of Mars. X_p (Eq. (5)) and Y_p (Eq. (6)) are two time-varying angles that position the pole of Mars crust with respect to its pole of rotation. The in-equatorial plane coordinates of $\Delta\vec{r}$ are modulated by the rover latitude only. Therefore, as it is commonly known, the higher in latitude the landed probe is, the larger will be the displacement of the rover in the equatorial plane due to PM. What is less known but shown in Eq. (12) is that the displacement of the landed probe along the polar axis, due to PM, is modulated by both the latitude and the longitude. Since the polar motion signature in the Doppler observables is proportional to $\Delta\vec{r}$, a similar dependence on the rover longitude is also clearly seen in the X_p and Y_p RMS contributions to the LOL/ROL Doppler measurements shown in Fig. 8. This figure shows in addition that these X_p and Y_p contributions are out-of-phase along the longitudes as suggested by the $\cos\lambda$ and $\sin\lambda$ in Eq. (12). One can therefore assumes that the decrease in uncertainty for the polar motion parameters is very dependent on both the longitude (λ) and latitude (φ) of the lander/rover.

Since we chose latitude ($\varphi = -2°$) and longitude ($\lambda = -6°$) of the rover both close to zero, the above equation indicates that the synthetic Doppler observables, proportional to $\Delta\vec{r}$, used in our simulations, are only affected by the X_p contribution to the rover position variations along the pole axis. As a consequence, for such a location of the rover at the surface of Mars, the Y_p component of the polar motion cannot be deter-

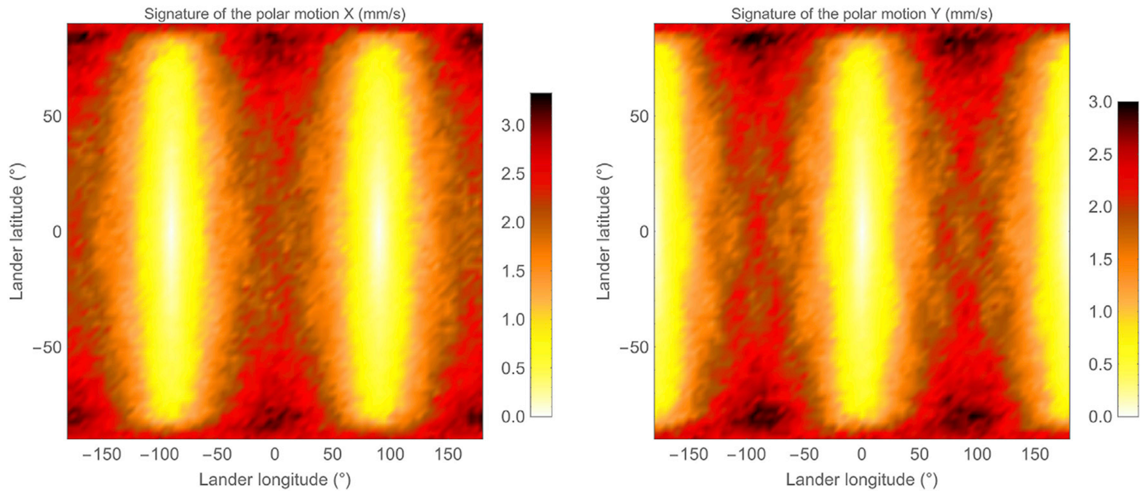

Fig. 8. Polar Motion signature in the LOL/ROL Doppler observables as a function of the lander/rover latitude and longitude. The drawn quantity is the quadratic mean of the observable temporal series over one martian year. Doppler unit is mm/s. The spacecraft has a quasi-polar (89°) precessing orbit at 500 × 500 km altitude.

mined. Moreover, since the X_p signature in the Doppler (up to 2 mm/s RMS at *Opportunity* landing site[8] given the PM model considered here) is well above the Doppler noise (0.05 mm/s in X-band and 0.3 mm/s in UHF for 60s integration time), this component of PM should be possible to improve from ROL data. Indeed, our simulations predict that Y_p uncertainties remain unchanged to their a priori value (not shown here) despite the large number of data accumulated over 700 days, whereas the precision on X_p obtained from ROL measurements should be better than 5 mas after one martian year of mission duration (see Fig. 9). In one hand, such a high precision in X_p remains large with respect to its expected annual and semiannual amplitudes (respectively at the 100–200% and 50–100% level of the model used to simulate the data, see Table 2). In the other hand, the Chandler amplitudes could be estimated at the 5% level, assuming the 33-mas-truth value considered here (see Table 2) as representative of the actual Martian Chandler wobble. Such a determination of the Chandler amplitudes would be powerful to constrain Mars interior and atmospheric models.

6. Rover-Orbiter-Earth triangular configuration

In this section, we briefly talk over the advantage of having both ROL and DTE tracking data simultaneously with the tracking of the orbiting spacecraft. We call this configuration as *triangular* because of the geometric figure drawn by the three links involved, namely the radio links between a landed probe, an orbiter, and a ground station on Earth (see Fig. 10). Such a configuration is planed in *ExoMars* program, and should be an ordinary configuration for the next space missions to Mars.

The triangular configuration has two main objectives:

(1) Lander/rover point of view: in order to better determine the MOP, one needs to precisely reconstruct the motion of the lander/rover in the inertial space. Since the Doppler data are functions of the relative velocity, i.e the velocity along the ray path, two Doppler links with different line-of-sight orientations would offer two complementary information about the velocity of the probe in 3D-space, allowing thereby to reduce the correlations between the adjusted parameters. The goal here is then to quantify the contribution of a second radio link in the landed probe motion computation and in the determination of the MOP.
(2) Orbiter point of view: in the same way, a second radio link between the lander/rover and the orbiter (in addition to the orbiter-Earth link) should clearly increase the precision of the orbit, permitting to better separate/understand/estimate each force acting on the spacecraft (the gravitational as well as the non-gravitational forces), and so to better determine the geophysical parameters of interest like gravity field or the tidal Love number, k_2.

The first objective is addressed here and the second one is not treated. Thus, focussing on the MOP determination, our simulations quantify the improvement afforded by the triangular data with respect to the isolated datasets. Fig. 5b displays the 1σ uncertainties evolution of the ΔLOD amplitudes as a function of the mission duration for each dataset separately (red, blue, green curves) and for a combination of ROL and DTE data (magenta and orange curves). We show that the triangular data always provide the best estimate precisions, with a more significant advantage when DTE and ROL (used separately) provide similar precision on the rotation parameters. In other words, the larger is the difference between DTE and ROL precisions in the MOP determination, the lesser useful is the triangular configuration. Indeed, as one can see on Fig. 5b, the triangular configuration is particularly interesting when combining DTE (red) and UHF-ROL (blue) datasets to estimate ϕ_2^c and ϕ_2^s (the semiannual amplitudes of ΔLOD). The combined precision being then (magenta) at the same level of precision as the one obtained by combining DTE with X-band-ROL datasets (orange). Compared to the separated DTE and UHF-ROL estimates, the triangular estimates (magenta) provide ΔLOD estimate precisions two times better than the best semiannual estimate precision inferred from the separated datasets. Such a gain on the determination of ϕ_2^c and ϕ_2^s would allow to slightly improve our knowledge on these parameters, not improved by the separated estimates. Although not shown on Fig. 6 (right panels), the same conclusion could be drawn for the nutation parameters p_2 and r_3 and, generally speaking, the exact same statements can be made for the lander case (i.e. with LOL data instead of ROL data).

7. Conclusion

In order to improve our knowledge on the Mars Orientation and rotation Parameters (MOP), we studied here what could be done with a radio-science experiment involving a long-life Martian rover equipped with a high performance mobility system as expected onboard *ExoMars*

[8] Note that the landing site candidates of *ExoMars 2020*) are Oxia Planum (333.2° E, 16.63° N) and Mawrth Vallis (342° E, 22° N). They are both in the vicinity of *Opportunity* and should thus enable to estimate X_p but not Y_p, similarly to what is shown here by our simulations.

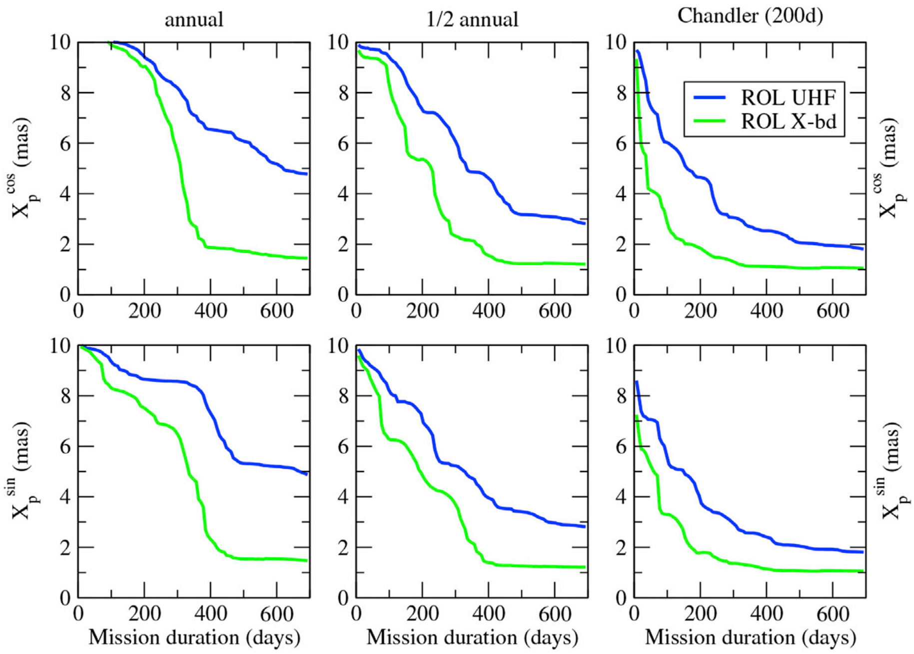

Fig. 9. Time evolution of the 1σ uncertainties in the Polar Motion X_p component estimated from the ROL Doppler measurements in UHF(blue) and in X-band (green). Since the rover is located at $\lambda = 354°$E of longitude and $\varphi = 2°$S of latitude, the uncertainties in Y_p component can not be improved and is thus not shown here (see detailed explanation in the text).. (For interpretation of the references to colour in this figure legend, the reader is referred to the Web version of this article.)

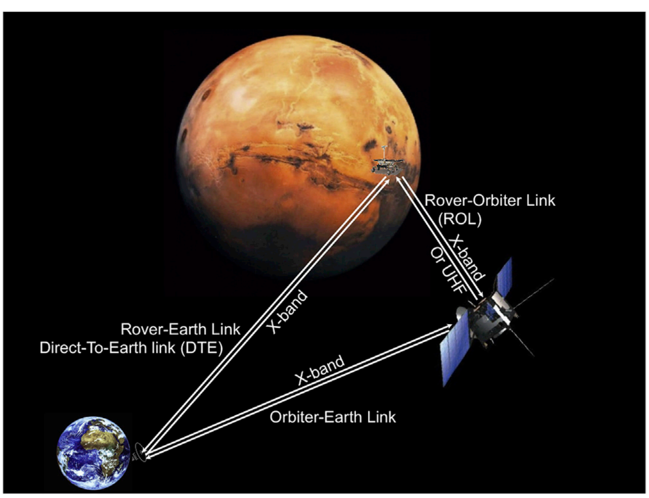

Fig. 10. Triangular configuration.

rover for instance. Such a mobility system should provide each successive rover position with 10 cm of accuracy relatively to the previous position. This level of relative positioning error is supported by the study of Winter et al. (2015), but further investigations and additional studies are needed to corroborate this assumption and get full confidence in the results presented here.

Assuming the initial position of the rover precisely determined in the inertial space from a commissioning phase of a few days, we have shown that the subsequent positions of the rover during tracking sessions can be determined with a precision of 10–100 cm in the inertial space (see Fig. 4) by using continuity constraints built from prior information provided by the mobility system. In such a case, we have shown that rover and lander data provide the same order of magnitude in precision on the Mars nutation parameters (see Fig. 6), while the Mars length-of-day variation parameters are significantly better estimated from lander data than from rover data (see Fig. 5). The impact of the current 1-m uncertainty in the orbiter trajectory have been shown to increase the uncertainties in the MOP determination by a factor of ten with respect to those obtained with a well-known orbiter trajectory. UHF radio link between the lander/rover and the orbiter (LOL/ROL) is found to provide comparable results to those obtained with Direct-To-Earth (DTE) link in X-band assuming the orbit determined at the meter level. We also emphasised the importance of the radio signal frequency used for the LOL/ROL link in the MOP determination, showing that the X-band results are two times better than UHF results. In addition, it is shown that the Rover-Orbiter-Earth triangular Doppler tracking data are helpful above all if both ROL and DTE datasets provide similar precision in the MOP determination when they are used separately. Finally, the polar motion and Chandler wobble amplitudes have been resolved in the ROL approach only, since DTE is insensitive to these parameters when the rover is close to the equator. The decrease in uncertainty for the polar motion parameters has been found to be very dependent on the latitude and longitude of the rover. Nevertheless, one of the two components (i.e. X_p or Y_p) should be determined with a precision better than 5 mas after one Martian year of operation, likely allowing for the first-ever direct measurement of the Martian Chandler Wobble signal.

Although the proposed radio-science experiment from a moving rover would barely improve the current precision on the MOP when processed alone, a combination of those Doppler data together with historical and future lander data would definitely help to decorrelate between the estimated parameters and consequently to reduce the uncertainties in the MOP estimates.

Acknowledgments

This work was financially supported by the Belgian PRODEX program managed by the European Space Agency in collaboration with the Belgian Federal Science Policy Office.

Appendix A. Supplementary data

Supplementary data related to this article can be found at https://doi.org/10.1016/j.pss.2018.03.020.

References

Barriot, J.-P., Dehant, V., Folkner, W., Cerisier, J.-C., Ribes, A., Benoist, J., van Hoolst, T., Defraigne, P., Warnant, R., Preston, R.A., Romans, L., Wu, S., Wernik, A.W., 2001. The netlander ionosphere and geodesy experiment. Adv. Space Res. 28, 1237–1249. https://doi.org/10.1016/S0273-1177(01)00295-2.

Defraigne, P., Dehant, V., Pâquet, P., December 1995. Link between the retrograde-prograde nutations and nutations in obliquity and longitude. Celestial Mech. Dyn. Astron. 62, 363–376. https://doi.org/10.1007/BF00692286.

Dehant, V., Folkner, W., Renotte, E., Orban, D., Asmar, S., Balmino, G., Barriot, J.-P., Benoist, J., Biancale, R., Biele, J., Budnik, F., Burger, S., de Viron, O., Häusler, B., Karatekin, Ö., Le Maistre, S., Lognonné, P., Menvielle, M., Mitrovic, M., Pätzold, M., Rivoldini, A., Rosenblatt, P., Schubert, G., Spohn, T., Tortora, P., van Hoolst, T., Witasse, O., Yseboodt, M., July 2009. Lander radioscience for obtaining the rotation and orientation of Mars. Planet. Space Sci. 57, 1050–1067. https://doi.org/10.1016/j.pss.2008.08.009.

Folkner, W.M., Yoder, C.F., Yuan, D.N., Standish, E.M., Preston, R.A., December 1997. Interior structure and seasonal mass redistribution of Mars from radio tracking of Mars pathfinder. Science 278, 1749–1751. https://doi.org/10.1126/science.278.5344.1749.

Folkner, W.M., Asmar, S.W., Dehant, V., Warwick, R.W., March 2012. The rotation and interior structure experiment (RISE) for the InSight mission to Mars. In lunar and planetary institute science Conference Abstracts, volume 43 of lunar and planetary inst. Technical Report, p. 1721.

Folkner, W.M., Dehant, V., Le Maistre, S., Yseboodt, M., Rivoldini, A., Van Hoolst, T., Asmar, S., Golombek, M., 2018. The rotation and interior structure experiment on the InSight mission to Mars. Space Science Reviews. Submitted.

Gregnanin, M., Bertotti, B., Chersich, M., Fermi, M., Iess, L., Simone, L., Tortora, P., Williams, J.G., December 2012. Same beam interferometry as a tool for the investigation of the lunar interior. Planet. Space Sci. 74, 194–201. https://doi.org/10.1016/j.pss.2012.08.027.

Harri, A.-M., Marsal, O., Lognonne, P., Leppelmeier, G.W., Spohn, T., Glassmeier, K.-H., Angrilli, F., Banerdt, W.B., Barriot, J.P., Bertaux, J.-L., Berthelier, J.J., Calcutt, S., Cerisier, J.C., Crisp, D., Dehant, V., Giardini, D., Jaumann, R., Langevin, Y., Menvielle, M., Musmann, G., Pommereau, J.P., di Pippo, S., Guerrier, D., Kumpulainen, K., Larsen, S., Mocquet, A., Polkko, J., Runavot, J., Schumacher, W., Siili, T., Simola, J., Tillman, J.E., January 1999. Network science landers for Mars. Adv. Space Res. 23, 1915–1924. https://doi.org/10.1016/S0273-1177(99)00279-3.

Kahn, R.D., Folkner, W.M., Edwards, C.D., Feb 1992. Position determination of a lander and rover at Mars with Earth-based differential tracking. Jet Propulsion Laboratory - interoffice memorandum 42 (108), 279–293.

Konopliv, A.S., Yoder, C.F., Standish, E.M., Yuan, D.-N., Sjogren, W.L., May 2006. A global solution for the Mars static and seasonal gravity, Mars orientation, Phobos and Deimos masses, and Mars ephemeris. Icarus 182, 23–50. https://doi.org/10.1016/j.icarus.2005.12.025.

Konopliv, A.S., Asmar, S.W., Folkner, W.M., Karatekin, Ö., Nunes, D.C., Smrekar, S.E., Yoder, C.F., Zuber, M.T., January 2011. Mars high resolution gravity fields from MRO, Mars seasonal gravity, and other dynamical parameters. Icarus 211, 401–428. https://doi.org/10.1016/j.icarus.2010.10.004.

Konopliv, A.S., Park, R.S., Folkner, W.M., August 2016. An improved JPL Mars gravity field and orientation from Mars orbiter and lander tracking data. Icarus 274, 253–260. https://doi.org/10.1016/j.icarus.2016.02.052.

Kuchynka, P., Folkner, W.M., Konopliv, A.S., Park, R.S., Le Maistre, S., Dehant, V., February 2014. New constraints on Mars rotation determined from radiometric tracking of the opportunity Mars Exploration rover. Icarus 229, 340–347. ISSN 0019-1035. https://doi.org/10.1016/j.icarus.2013.11.015.

Le Maistre, S., November 2013. The Rotation of Mars and Phobos from Earth-based Radio-tracking Observations of a Lander. PhD thesis. Université Catholique de Louvain.

Le Maistre, S., February 2016. InSight coordinates determination from direct-to-Earth radio-tracking and Mars topography model. Planet. Space Sci. 121, 1–9. https://doi.org/10.1016/j.pss.2015.11.003.

Le Maistre, S., Rosenblatt, P., Rivoldini, A., Dehant, V., Marty, J.-C., Karatekin, Ö., July 2012. Lander radio science experiment with a direct link between Mars and the Earth. Planet. Space Sci. 68 (1), 105–122. https://doi.org/10.1016/j.pss.2011.12.020. ISSN 0032-0633.

Marty, J.C., Balmino, G., Duron, J., Rosenblatt, P., Le Maistre, S., Rivoldini, A., Dehant, V., van Hoolst, T., March 2009. Martian gravity field model and its time variations from MGS and Odyssey data. Planet. Space Sci. 57, 350–363. https://doi.org/10.1016/j.pss.2009.01.004.

Roosbeek, F., 1999. Analytical developments of rigid Mars nutation and tide generating potential series. Celestial Mech. Dyn. Astron. 75, 287–300.

Rosenblatt, P., Marty, J.C., Perosanz, F., Barriot, J.P., van Hoolst, T., Dehant, V., September 2004. Numerical simulations of a Mars geodesy network experiment: effect of orbiter angular momentum desaturation on Mars' rotation estimation. Planet. Space Sci. 52, 965–975. https://doi.org/10.1016/j.pss.2004.07.017.

T. Sasao, S. Okubo, and M. Saito. A simple theory on the dynamical effects of a stratified fluid core upon nutational motion of the earth. In Nutation and the Earth's Rotation; Proceedings of the Symposium, Kiev, Ukrainian SSR, May 23-28, 1977. (A80-45776 19-46) Dordrecht, D. Reidel Publishing Co., vol. 1980, p. 165–183., pages 165–183, 1980.

Van den Acker, E., Van Hoolst, T., de Viron, O., Defraigne, P., Forget, F., Hourdin, F., Dehant, V., July 2002. Influence of the seasonal winds and the CO_2 mass exchange between atmosphere and polar caps on Mars' rotation. J. Geophys. Res. B 107, 5055. https://doi.org/10.1029/2000JE001539.

Van Hoolst, T., December 2007. The rotation of the terrestrial planets. In: Spohn, T., Schubert, J. (Eds.), Treatise of Geophysics: `Planets and Moons, vol. 10. Elsevier Publ., pp. 123–164

Van Hoolst, T., Dehant, V., Defraigne, P., 2000a. Sensitivity of the free core nutation and the Chandler wobble to changes in the interior structure of Mars. Phys. Earth Planet. In. 117, 397–405.

Van Hoolst, T., Dehant, V., Defraigne, P., 2000b. Chandler wobble and free core nutation for Mars. Planet. Space Sci. 48, 1145–1151.

Van Hoolst, Tim, Rivoldini, Attilio, 2014. Interior structure and evolution of Mars. In: Spohn, Tilman, Breuer, Doris, Johnson, Torrence V. (Eds.), Encyclopedia of the Solar System, 3 edition. Elsevier Inc., pp. 379–396 (chapter 18).

Winter, M., Barcaly, C., Pereira, V., Lancaster, R., Caceres, M., McManamon, N.B., Silva, N., Lachat, D., Campana, M., May 2015. ExoMars Rover vehicle: detailed description of the GNC system. In: Astra. ESTEC.

Yseboodt, M., Barriot, J.-P., Dehant, V., July 2003. Analytical modeling of the Doppler tracking between a lander and a Mars orbiter in terms of rotational dynamics. J. Geophys. Res. B 108, 5076. https://doi.org/10.1029/2003JE002045.

Yseboodt, M., Dehant, V., Iess, L., Mitrovic, M., Gregnanin, M., September 2012. Same beam interferometry on Mars for obtaining information on the interior. In: European Planetary Science Congress 2012, p. 522.

Yseboodt, Marie, Dehant, Véronique, Péters, Marie-Julie, 2017. Signatures of the martian rotation parameters in the Doppler and range observables. Planet. Space Sci. 144, 74–88. ISSN 0032-0633. https://doi.org/10.1016/j.pss.2017.05.008.

Zuber, M.T., Lemoine, F.G., Smith, D.E., Konopliv, A.S., Smrekar, S.E., Asmar, S.W., May 2007. Mars reconnaissance orbiter radio science gravity investigation. J. Geophys. Res. B 112. https://doi.org/10.1029/2006JE002833. E05S07.